HHS Public Access

Author manuscript

Dev Cell. Author manuscript; available in PMC 2018 December 04.

Published in final edited form as:

Dev Cell. 2017 December 04; 43(5): 577–587.e5. doi:10.1016/j.devcel.2017.10.030.

Bleb expansion in migrating cells depends on supply of membrane from cell surface invaginations

Mohammad Goudarzi[1], **Katsiaryna Tarbashevich**[1], **Karina Mildner**[2], **Isabell Begemann**[3], **Jamie Garcia**[4], **Azadeh Paksa**[1], **Michal Reichman-Fried**[1], **Harsha Mahabaleshwar**[1], **Heiko Blaser**[5], **Johannes Hartwig**[1], **Dagmar Zeuschner**[2], **Milos Galic**[3], **Michel Bagnat**[4], **Timo Betz**[1], and **Erez Raz**[1,6,*]

[1]Institute for Cell Biology, ZMBE, Von-Esmarch-Street 56, 48149 Münster, Germany

[2]Electron Microscopy Unit, Max Planck Institute for Molecular Biomedicine, Röntgenstr. 20, 48149 Münster, Germany

[3]Workgroup Nanoforces in Cells, Institute of Medical Physics und Biophysics, DFG Cluster of Excellence 'Cells in Motion', (EXC 1003), Robert-Koch-Str. 31 48149 Münster, Germany

[4]Department of Cell Biology, 333B Nanaline Duke Bldg., Box 3709 Duke University, Durham, NC 27710, USA

[5]Germ Cell Development, Max-Planck-Institute for Biophysical Chemistry, Am Fassberg 11, 37070 Göttingen, Germany

Abstract

Cell migration is essential for morphogenesis, for organ formation and homeostasis, with relevance for clinical conditions. The migration of primordial germ cells (PGCs) is a useful model to study this process in the context of the developing embryo. Zebrafish PGC migration depends on the formation of cellular protrusions in form of blebs, a type of protrusion found in various cell types. Here we report on the mechanisms allowing the inflation of the membrane during bleb formation. We show that the rapid expansion of the protrusion depends on membrane invaginations that are localized preferentially at the cell front. The formation of these invaginations requires the function of Cdc42, and their unfolding allows bleb inflation and dynamic cell-shape changes performed by migrating cells. Inhibiting the formation and release of the invaginations strongly interfered with bleb formation, cell motility and with the ability of the cells to reach their target.

[*]Correspondence should be addressed to E.R. (erez.raz@uni-muenster.de).

[6]Lead Contact: Erez Raz, Institute for Cell Biology, ZMBE, Von-Esmarch-Street 56, 48149 Münster, Germany, erez.raz@uni-muenster.de

AUTHORS CONTRIBUTION

Mohammad Goudarzi performed all the experiments except for the followings: K.M. and D.Z. Performed the electron microscopy studies. K.T. performed experiments examining the possible involvement of BAR-domain containing proteins in bleb formation. A.P. designed probes and performed the two-color *in situ* hybridization. H.B. generated the VAMP8 and Exo70 plasmids. M.R. designed the Exo70 and designed and generated the Cdc42 plasmid. H.M. designed and constructed the Rab5c and Rab11a plasmids. I.B. and M.G. designed and constructed the Amphiphysin and Nadrin plasmids. M.B. and J.G. performed the experiments involving the caveolin mutant embryos. J.H designed and constructed the CLIP170 plasmid. T.B. analyzed experiments relevant for membrane flow. E.R. participated in all the experimental design and guidance. All authors contributed to writing of the manuscript and M.R edited and critically read multiple versions of the manuscript.

Keywords

Cell migration; Zebrafish; Primordial germ cells; PGC; membrane; Bleb; N-BAR

INTRODUCTION

Protrusion in motile cells can be formed by polarized actin polymerization at the cell front or by hydrostatic pressure generated in the cytoplasm by the contractile actomyosin cortex (Charras and Paluch, 2008; Paluch and Raz, 2013; Small et al., 2002) (Diz-Munoz et al., 2016; Friedl and Wolf, 2010) (Fackler and Grosse, 2008; Welch, 2015). Blebs are generated in regions of the cell circumference where the plasma membrane detaches from the cell cortex or at locations where membrane-to-cortex attachment is reduced. Such "weak spots" can result from local reduction in the level of molecules such as ezrin/radixin/moesin (Fehon et al., 2010; Paluch and Raz, 2013), or as a consequence of an increase in local contractility of the cell cortex (Keller and Eggli, 1998; Paluch et al., 2005). Certain models describing cell shape changes during protrusion formation assume that the cell volume is preserved and generally consider the plasma membrane to behave as a flat elastic substance (Kabaso et al., 2011; Strychalski and Guy, 2013). In a recent study however, Taloni *et al.* suggest that protrusion formation involves an increase in cell volume and surface (Taloni et al., 2015), further highlighting the need for a membrane source for the bleb formation. Since stretching of a flat plasma membrane just prior to its rupture is limited to 2–3% (Kleinschmidt, 2006; Kwok and Evans, 1981; Sheetz et al., 2006) and given that the force needed for such expansion is 2–3 orders of magnitude greater than the force cells can generate (Sheetz et al., 2006), the question that arises concerns the source of the additional membrane required for bleb inflation.

Here we used primordial germ cells (PGCs) that migrate through the developing embryo (Barton et al., 2016) as an *in vivo* model for investigating the cellular mechanisms contributing to protrusion formation in single cell migration. We find that the rapid expansion of the bleb-type protrusions in zebrafish PGCs depends on invaginations found around the cell circumference. Unfolding of these structures provides the membrane for protrusion inflation in the direction of cell migration.

RESULTS

During the first day of embryonic development, zebrafish primordial germ cells (PGCs) migrate from the positions at which they are specified towards the region where the gonad develops (Barton et al., 2016; Paksa and Raz, 2015). The migrating zebrafish PGCs can be visualized within the developing embryo by expression of fluorescent protein fusions that label specific cellular structures (Blaser et al., 2005; Kardash et al., 2010). It was shown that as PGCs migrate in live embryos, they extend bleb-type protrusions (Blaser et al., 2006; Goudarzi et al., 2012). Bleb expansion is characterized by rapid flow of cytoplasm driven by hydrostatic pressure, leading to outward deformation of the cell membrane (Paluch and Raz, 2013). Despite the importance of blebs for cell migration and their prevalence in other

processes (e.g. apoptosis and cell division), experimental data concerning the source of membrane required for bleb growth is still lacking (Paluch and Raz, 2013).

The rapid inflation of the bleb requires a local membrane source

As the first step in studying the cellular mechanisms underlying bleb formation, we measured the cell surface area, volume and membrane fluorescence intensity during blebbing of PGCs whose membrane was labeled with farnesylated EGFP. The surface and volume were analyzed using 3D reconstructions of spinning disk microscopy stacks by the Imaris software (Bitplane) employing the surface function for Bleb and Pre-Bleb time points. The fluorescence intensity at the membrane was quantified, employing a three-step Radial Analysis program (see Methods): 1) identification of cell contours (segmentation) 2) Determination of the distance between the cell edge and it center around the cell perimeter. 3) Identification of maximal fluorescence in 10 pixel areas around the cell edge. Blebs were located in a Postprocess step (see Methods) by identifying areas with dynamic shape alterations.

As presented in Figure 1A, the apparent cell surface area and volume of cells did not change as a result of bleb expansion. We next measured the cell circumference at the region of the bleb and at the rest of the cell, before and after bleb inflation (Figure 1B, left). This analysis revealed a substantial increase in the perimeter of the bleb region upon bleb inflation (Figure 1B, right). Indeed, this increase can also be observed in a 3D presentation, where the surface area of the bleb and that of the whole cell are measured before and after bleb inflation (an example is shown in Figure 1C). Interestingly, using the Radial analysis and Postprocess programs that allow for detection of cell outline and signal evaluation in cells undergoing dynamic shape alterations (see Methods), we noticed a local reduction in membrane-associated EGFP intensity in the bleb region during bleb expansion (Figure 1D).

These observations are consistent with the assumption that bleb formation is a local event, and does not involve transfer of material towards the protrusion. To examine this hypothesis further, we photoconverted a farnesylated Dendra2 protein (Dendra2-F) at the vicinity of a forming bleb (Figure 2A) and monitored the position and shape of the photoconverted area. Despite the technical difficulties associated with this manipulation in deep layers of the embryo and the fact that the precise position where blebs form is unknown prior to their expansion, we were able to photoconvert the membrane-targeted Dendra2 protein very close to and even at the edge of forming blebs. By following the edge velocity of the converted area relative to the bleb, we sought to determine whether bulk flow of membrane towards the bleb could be observed. Interestingly, as the bleb expanded no directed flow of the converted Dendra (red) could be observed (Figure 2A middle and lower panels, Movie S1A). Additionally, the spread of the converted Dendra2-F (red) signal during the experiment was symmetrical relative to its center (see intensity profile in Figure 2B) and similar between blebbing and non-blebbing cells (Figure 2C). Measuring the intensity allowed tracking the lateral velocity of the center of the photoconverted area, which was found to be close to 0 independent of whether a bleb formed or not (Figure 2C), with a diffusion rate of the fluorescent proteins (1.8 μm/sec, measured at the edge of the converted area, see Methods section) similar to that previously described for other membrane-bound proteins (e.g. D=1.7

± 0.22 $\mu m^2/s$ for GFP labeled plextrin-homology domain of PLCδ1 (PHδ1) (Goehring et al., 2010)). Consistent with photoconversion experiments, photobleached areas located next to a forming bleb showed no displacement towards the region of membrane inflation (Figure S1A, Movie S1B). Last, photobleached regions located within the inflating bleb showed local expansion upon bleb growth with only limited signal diffusion from the rest of the cell (with the fluorophore fused to a farnesylation signal, Figure S1B, Movie S1C, or to a truncated non-internalizable 7-transmembrane Cxcr4b receptor respectively, Figure S1C). Together, the results of these *in vivo* experiments are consistent with the idea that a local supply of membrane supports bleb expansion. Nevertheless, as the analysis presented above relied on monitoring fluorescent proteins, the formation of the bleb could depend on lipid flow or fusion of vesicles that do not contain the labeled membrane marker.

To investigate the possibility that lipid flow supports bleb expansion, we exposed isolated PGCs to the lipid dye FM4-64, thereby labeling lipids in the outer leaflet of the plasma membranes. Normal blebs that formed occasionally by the dissociated PGCs (in contrast to the more common travelling “circus blebs” that form under these conditions (Charras et al., 2008)) showed reduced plasma membrane label intensity at the tip of blebs (Figure S1D, E). The non-homogenous distribution of the lipid dye fluorescence (Figure S1D) is consistent with the idea that the plasma membrane is not a flat structure but rather contains wrinkles. Together, our data do not support the notion that lipid or membrane-anchored proteins flow into the forming bleb, but instead suggest that local membrane supply supports bleb inflation.

Membrane invaginations act as a source for plasma membrane in blebbing cells

Structures such as filopodia and caveolae could potentially constitute a membrane reservoir required for bleb expansion. Along these lines, it has been previously shown that filopodia are more abundant at the front of migrating PGCs (Meyen et al., 2015), the site at which blebs occur more frequently (Reichman-Fried et al., 2004). However, we observed that when blebs inflated, the average length of nearby filopodia remained unaltered (Figure S2), suggesting that these structures do not contribute membrane material to the bleb. We subsequently examined other potential membrane-storing structures that could contribute membrane to the inflating bleb.

Caveolae are small (50–100 nm in diameter) membrane invaginations that contain proteins and lipids including caveolins (Nassoy and Lamaze, 2012; Sinha et al., 2011). In mouse lung endothelial (Sinha et al., 2011) and muscle cells (Gervasio et al., 2011), caveolae were shown to buffer membrane tension in response to physical stretch. Caveolin-1 (Cav1) protein plays an essential role in caveolae formation in non-muscle tissues (Drab et al., 2001; Sinha et al., 2011) and its mRNA is uniformly expressed in early zebrafish embryo including the PGCs (Figure S3A). To follow the distribution of the protein within the PGCs, we expressed Cav1a-GFP fusion protein in the embryo and followed its localization. As shown before (Arbizzani et al., 2015), the Cav1a-GFP marks the membrane in certain lineages of the somatic cells (Figure S3B). Interestingly, in migrating PGCs, Cav1-GFP is primarily localized to structures in the vicinity of the plasma membrane at the back of the migrating cells, sub-cellular localization that appeared inconsistent with a role in bleb formation

(Figure S3B). Nevertheless, we proceeded to examine PGC behavior in mutant embryos lacking the maternal and zygotic of both Cav1 and Cav3 proteins, mutants in which caveolae formation and function are severely impaired, such that they are strongly reduced in number (Cao et al., 2016; Garcia et al., 2017). In these experiments, despite the lack of both caveolin proteins, we observed no effect on either bleb expansion or on the ability of the cells to actively migrate and reach their target (Figure S3C, Movie S2). Together, employing the available tools for an *in vivo* analysis, our data argues against a significant role for caveolae in bleb formation.

We next examined whether vesicles could serve as a local membrane source for bleb expansion. Vesicles were previously shown to be important for the migration of different cell types by allowing the transport of relevant molecules to the membrane and by providing membrane material (Hopkins et al., 1994) (Spiczka and Yeaman, 2008) (Zanchi et al., 2010). To examine the possibility that polarized deposition of vesicles contributes to bleb expansion, we determined the position of the Golgi apparatus, which we found to be localized away from the cell front (Figure S4A, left panel). We then examined the possible role of the exocyst complex (Inoue et al., 2003), early endosomes (Chavrier et al., 1990) and recycling vesicles (Takahashi et al., 2012) in bleb formation. Fluorescently-tagged Endobrevin (VAMP8) and Rab11a showed localization at the back of the cells (Figure S4A, middle and right panels), while tagged Rab5c and Exo70 proteins were found in uniformly distributed vesicles (Figure S4A, bottom panels). Towards clarifying the role of vesicles in blebbing, we expressed high levels of previously described dominant-negative forms of the Exo70 (Inoue et al., 2003), Rab11a (Ren et al., 1998) and Rab5c (Stenmark et al., 1994). The dominant negative proteins were expressed either in all cells of the embryo or specifically in the PGCs. While global expression adversely affected embryonic development, reflecting efficient inhibition of the protein function (Figure S4B, global DN expression), preferential expression in PGCs neither affected the ability of cells to reach their migration target (Figure S4B, DN expression in PGCs) nor blebbing rates (Figure S4C), supporting the idea that Exo70, Rab11a and Rab5c function is not essential for this process. Together, these results are consistent with the idea that vesicle transport and recycling do not play a major role in bleb formation.

Another potential source for membrane material supporting bleb expansion are invaginations of the plasma membrane. The involvement of such invaginations in bleb inflation was previously hypothesized (Sens and Plastino, 2015). Indeed, membrane unfolding was suggested to fuel cell-surface growth in the context of cellularization of *Drosophila* embryos (Figard et al., 2016; Figard et al., 2013) and for increasing the apparent cell surface area in the context of osmotic swelling and phagocytosis (Hallett and Dewitt, 2007). In the case of bleb formation *in vitro*, in trypsinated CHO and NIH3T3 cells that form “travelling” non directional oscillating blebs, membrane invaginations were observed (Kapustina et al., 2013). However, the relevance and role of such structures for polarized bleb formation and their importance for cell migration in the physiological context of the live organism has never been addressed.

Intriguingly, examining PGCs within live embryos, we could observe dynamic inwards-pointing membrane indentations (Movie S3A). Interestingly, invaginations that appear

similar to the structures we detected were described in other cell types that lack caveolae, i.e. in yeast cells. These invaginations termed eisosomes (Karotki et al., 2011) were found to be essential for rapid membrane expansion upon osmotic shock (Kabeche et al., 2015). Detailed characterization of the PGCs in fixed embryos confirmed the presence of such inward extensions (Figure 3A, red arrowhead). The membrane invaginations often appeared as disconnected structures whose link to the plasma membrane could be traced through optical sections (Figure 3A, red arrowheads, Movie S3B). Importantly, such structures could not be observed within blebs, suggesting that they unfolded and provide membrane material for bleb inflation (e.g., see Movie S3A). This phenomenon could be clearly demonstrated in fixed cells following an increase in contractility within the PGCs by overexpression of a constitutively active form of myosin light chain kinase (CA-MLCK) (Blaser et al., 2006) (Figure 3B). In this case, the unusually large blebs induced by expression of CA-MLCK were mostly devoid of such membrane structures and the number of overall invagination detected in the cells was dramatically reduced (Figure 3B).

Additionally, plasma membrane invaginations could be observed by electron microscopy on ultrathin sections. These invaginations were detected in the context of the tissue by laser-mark assisted Correlative Transmission Electron Microscopy (TEM) (Goudarzi et al., 2015) and by Teneo VolumeScope (VS) serial block-face electron microscope (FEI™) (Figure 3C, D). Although in these experiments with fix material we could not define the polarity of the cells, we confirmed the presence of membrane invaginations along the surface of PGCs. Quantifying the amount of sub-optical resolution wrinkling over the whole surface of two PGCs using the Teneo VS™ electron microscope (Figure 3C, Movie S3C) we found that the measured cell circumference is significantly larger than that measured in a line that excludes the EM-detected invaginations (35% and 25% in the two examples in Figure 3D). Importantly, these measurements are an underestimate, as invaginations were not followed through multiple planes. Nevertheless, they are in the range of the measured length difference between the pre-bleb and post-bleb (ca. 50% for length expansion), suggesting that they provide a very significant amount of material needed for bleb expansion.

To directly investigate the role of membrane invaginations in bleb formation, we followed their dynamics by expressing BAR domains as curvature sensors (Frost et al., 2009). These BAR domains can sense curvatures that are induced by external push or internal pull (Galic et al., 2012). We found that N-BAR domains of Amphiphysin and Nadrin labeled dynamic invaginations at the circumference of the cell (Movie S4A and S4B respectively) and used the N-BAR domain of Amphiphysin (hereafter referred to as Amph-N-BAR-YFP) in the following experiments. At the protein level used (e.g., 50pg of a Amph-N-BAR-YFP per embryo) no effect on blebbing or migration was observed, such that we considered the reagent to serve merely as a sensor. It is only when 5-fold amounts were used that inhibition of protrusion formation was observed (Figure S5). Strikingly, the fusion protein was found to be distinctly localized to the plasma membrane (Figure 4A). Expression was particularly prominent at the leading edge of migrating cells where dynamic changes in cell shape and blebbing occur (Movie S4C). Thus, these results confirm the presence of invaginations along the cell surface of PGCs and are consistent with their involvement in the process of blebbing. In addition, when compared with a farnesylated form of the mCherry protein, the fluorescence intensity level of Amph-N-BAR-YFP was more dramatically reduced during

bleb expansion and was markedly enhanced during bleb retraction (Figure 4A and 4B, Movie S4C). Together, these observations are in line with the idea that during bleb expansion membrane invaginations are flattened and reform in the course of bleb retraction.

The data presented above suggest that rapid release of membrane material from the invaginations allows bleb inflation in the context of the live embryo. To examine this point in a different setup, we exposed PGCs in a disrupted embryo to hypo-osmotic conditions inducing water influx and observed the disappearance of the Amph-N-BAR-YFP-marked membrane invaginations (Figure 4C, left panel and graph, first part of Movie S5). Conversely, exposing the embryos to hyper-osmotic medium resulted in reformation of the invaginations in the PGCs and restoration of the blebbing activity (Figure 4C, right panel and the second part of Movie S5).

Membrane unfolding is essential for bleb formation and cell migration

As a first step in determining whether membrane unfolding is of functional importance for bleb formation, we examined their localization relative to other structures. As shown in Figure 5A, microtubules and the microtubules organizing center were localized primarily to the back of the cell and did not show co-localization with Amph-N-BAR-YFP. In contrast, we observed strong co-localization between the BAR-domain-labeled invaginations and labeled actin (Fig 5B, cell front facing the microscope objective). Importantly, the invaginations labeled by Amph-N-BAR-YFP were concentrated at the front of the cell where the actin signal was elevated due to the presence of actin-rich structures (Figure 5C) (Kardash et al., 2010). To determine whether actomyosin contractility is required for the generation of the invaginations, we expressed a dominant negative form of Rho kinase (DN-ROCK) in PGCs (Blaser et al., 2006). In cells expressing DN-ROCK membrane invaginations continued to form at the cell front (Figure 5D). Consistent with the idea that bleb formation is coupled with the release of membrane from invaginations, expression of constitutively-active myosin light chain kinase (CA-MLCK) that elevated contractility led to the formation of large blebs devoid of invaginations (Movie S4D).

Interestingly, similar to our observations, invaginations whose formation does not depend on caveolae were described before in yeast where they function as membrane stores (Kabeche et al., 2015; Karotki et al., 2011), and as part of the CLIC/GEEC endocytosis pathway (Sabharanjak et al., 2002) which is controlled by the actin regulator Cdc42 (Heasman and Ridley, 2008; Mayor et al., 2014). Remarkably, expressing a dominant negative form of Cdc42 (DN-Cdc42, N17) (Akeda et al., 2002) in the germ cells led to round cell morphology, decreased formation of the membrane invaginations and reduced blebbing (Figure 5E, Movie S6). This observation is consistent with the notion that membrane invaginations essential for bleb formation depend on actin for their formation. Importantly, relative to controls, a significantly larger number of the manipulated cells failed to reach their target by the end of the first day of development (Figure 5F).

While BAR-domains serve as sensors for membrane curvature, at a high concentration they stabilize or even induce membrane invaginations (Frost et al., 2009; Peter et al., 2004). Expressing high levels Amph-N-BAR-YFP in the PGCs (250pg) (Figure S5) resulted in an increase in membrane invaginations (Figure 6A) and their persistence (Figure 6A, graph).

Strikingly, this manipulation led to a gradual decrease in blebbing activity along with cell rounding (Figure 6B, Movie S4E). Indeed, cells expressing high levels of the Amph-N-BAR-YFP largely failed to reach their migration target (Figure 6C), without an effect on their viability as judged by the presence of the cells in older (48hpf) embryos (Figure 6C).

DISCUSSION

The results reported in this study provide evidence for the presence of distinct membrane invaginations at the leading edge of blebbing cells and demonstrate their role in bleb formation and migration in the context of a live embryo. Our results show that cells use those structures for rapid local changes in the surface area needed for protrusion formation and retraction. In the course of bleb expansion, the invaginations are ironed out and subsequently reformed when blebs retract. Inhibiting the formation or the unfolding of these structures resulted in inhibition of bleb generation and PGC migration.

According to Taloni *et al.*,(Taloni et al., 2015) aquaporin-dependent water influx is responsible for bleb expansion in PGCs, in a process that involves an increase in cell volume. Employing fast microscopy instrumentation to achieve high z-axis resolution and using a different approach in volume rendering we reached to a different conclusion i.e. we could not detect a substantial change in cell volume or cell surface correlated with protrusion formation (a reduction of 3% on average in cell volume and no change in average cell surface area Figure 1A, (Blaser et al., 2006)). Consistently, following the intensity of a cytoplasmic fluorescence protein we do not detect a reduction in signal upon protrusion formation arguing against water influx (Figure S6).

We propose that the role of the membrane invaginations is to provide material allowing rapid reduction in membrane tension and fast expansion of blebs. We show that in polarized cells these membrane invaginations and actin-rich structures co-localize at the cell front and assume that their rapid release in the course of bleb expansion can be considered passive as shown in *in vitro* setting in a different context (Kosmalska et al., 2015). The local association between invaginations and the actin could be extended to a functional link, as disruption of Cdc42 adversely affects membrane invagination formation and culminates in abnormal cell shape and impaired migration.

We suggest that vesicle fusion, caveolae and filopodia are not essential sources for membrane material in the context of bleb inflation, but the level of accuracy of this analysis does not rule out the option that these and other membrane sources contribute to some extent to the process. Direct tests for the model we propose would require the use of methods such as atomic force microscopy or optical tweezers-mediated membrane tether pulling, while monitoring the effect on folds in the plasma membrane.

Rather, we show that transient invaginations play this role. While we study Zebrafish PGC migration, the presented results could be relevant for other cells types that generate blebs for their migration (e.g.(Lammermann and Sixt, 2009),(Diz-Munoz et al., 2016)), as well as for other cellular events where blebs are found (e.g., (Norman et al., 2010),(Laster and Mackenzie, 1996). It would also be interesting to determine if the distribution or the

dynamics of such invaginations are altered upon the transition between lamellipodia and bleb-driven migration in cells that can switch between the two modes of protrusion formation (Diz-Munoz et al., 2016; Driscoll and Danuser, 2015; Friedl and Wolf, 2010; Welch, 2015).

Last, in addition to their relevance for bleb formation in a range of contexts, the results presented here are relevant for other processes where rapid addition of membrane is required. For example, cellularization in *Drosophila* was shown to involve membrane unfolding to fuel cleavage furrow ingression (Figard et al., 2016; Figard et al., 2013), similar to lamellipodia extension where folds were implicated as well (Gauthier et al., 2011), and in phagocytosis where membrane folds provide the membrane area required for pseudopod extension (Masters et al., 2013). Comparing the molecular composition and dynamics of these structures in different cell types will shed light on the mechanisms responsible for their formation and the control over their release in the different cellular processes involving rapid membrane expansion.

STAR METHODS

CONTACT FOR REAGENT AND RESOURCE SHARING

Further information and requests for resources and reagents should be directed to and will be fulfilled by the lead contact, Erez Raz (erezraz@uni-muenster.de).

EXPERIMENTAL MODEL AND SUBJECT DETAILS

Zebrafish Strains—Zebrafish (*Danio rerio*) of the AB background and transgenic fish carrying the *Tg(kop:EGFP-f-UTRnanos3)* expressing EGFP on the membrane of PGCs as a result of maternal expression of mRNA that includes the *nanos3* untranslated region (Blaser et al., 2005), *Tg(kop:mCherry-f-UTRnanos3)* expressing mCherry on the membrane of PGCs as a result of maternal expression of mRNA that includes the *nanos3* untranslated region (Tarbashevich et al., 2015) and *Tg(kop:EGFP-LIFEACT-UTRnanos3)* expressing EGFP-lifeact protein that labels actin structures in PGCs as a result of maternal expression of mRNA that includes the *nanos3* untranslated region (Meyen et al., 2015) were used as wild-type fish. *cav1;cav3* mutants fish were previously described (Cao et al., 2016; Garcia et al., 2017). Briefly, the $cav1^{1104}$ mutants were generated using TALEN pairs to target to the common sequence of both *cav1* isoforms, leading to a 23nt deletion and the $cav3^{pd1149}$ mutant allele was generated using two CRISPRs that remove a 765-bp region between exon 1 and intron 1, resulting in the deletion of 90 bp of coding sequence. Zebrafish were maintained on a 14-hour light/10-hour dark cycle, and fertilized eggs were collected and raised at 25.1°C, 27.7°C or 32°C. Embryos were kept in 0.3× Danieau's solution [17.4mM NaCl, 0.21mM KCl, 0.12mM $MgSO_4{\cdot}7H_2O$, 0.18mM $Ca(NO_3)_2$, 1.5mM HEPES (pH 7.6)]. The embryos used were of early developmental stages, precluding determination of the sex of the animals. The general fish maintenance at the Institute follows the regulations of the LANUV NRW and is supervised by the veterinarian office of the city of Muenster.

METHOD DETAILS

RNA Expression, Constructs and Injections—mRNA was synthesized using the mMessage Machine kit (Ambion). RNAs were injected into the yolk of one-cell stage or into one of the eight blastomeres of the 8-cell stage embryo embryos. The experimental and control embryos were from same clutch of eggs.

For a list of the RNA-expression constructs used see the “KEY RESOURCES TABLE”.

Spinning Disk (SD) microscopy—Embryos were imaged using Carl Zeiss Axio imager Z1 microscope equipped with Yokogawa csu10B spinning disk. Samples maintained at 28°C using heated stage (PECON, TempController 2000-2). Imaging was performed using Cascade camera and Visitron Systems acquisition software (Visi-View 2007–2011). A 405nm laser was employed in bleaching and photoconversion experiments.

Volume and Surface area measurement—PGCs from 7–8hpf *Tg(kop:mCherry-f-UTRnanos3)* transgenic line were imaged using a spinning disk microscope with 1 μm difference between z-planes and 2 sec time intervals between stacks. 3D reconstructions were generated using the Imaris software (Bitplane) employing the surface function for Bleb and Pre-Bleb time points.

Cell circumference measurement—PGCs in embryos from the *Tg(kop:EGFP-f-UTRnanos3)* line were imaged by Spinning Disk microscopy at 7 hpf at a rate of one Z-stack per 2 seconds with 1 μm optical sections. During analysis, the plane of bleb inflation was selected and the change in the cell circumference in the bleb region and the rest of the cell was measured using the freehand tool of the Fiji software. The expression of the fluorescent protein on the PGC membrane was achieved using mRNA that includes the *nanos3* untranslated region (Blaser et al., 2005).

Change in signal intensities during bleb expansion—The cell contour was defined using a custom-made program (Radial analysis, http://dx.doi.org/10.17632/wmtzc7w3d7.2) based on thresholding the intensity of the plasma membrane labeled with fluorescent protein (EGFP-F). Blebs were identified using “postprocess_analysis” software (http://dx.doi.org/10.17632/wmtzc7w3d7.2) based on the velocity of the plasma membrane, manually validated and the intensity of the central half of the bleb was plotted over time (red dashed line in the Fig. 1D).

Photoconversion—Embryos of the AB background were injected at 1-cell stage with 50pg of *dendra2-f-nanos3-3′ UTR* mRNA, leading to expression of the Dendra2-F protein on the membrane of the PGCs. At 7–8hpf a selected region on the plasma membrane of PGCs was irradiated using a 405nm laser at 5% of the power, converting Dendra2-F molecules from green to red.

Analysis of lateral mobility of photoconverted area—Following photoconversion, images of the green (unconverted) and red (converted) channel were recorded with a time-resolution of 1s per time point. The cell perimeter was detected using thresholding and the photoconverted intensity was measured (Figure 2B) as function of the perimeter and angle.

To describe the diffusion we followed a recently developed model (Goehring et al., 2010) to gain a fit function for the 1D intensity profile of the photoconverted region:

$$I(t; x_1, x_2) = I_{bg} + \frac{b}{2}\left[\mathrm{erf}\left(\frac{x - x_2}{\sqrt{2Dt}}\right) - \mathrm{erf}\left(\frac{x - x_1}{\sqrt{2Dt}}\right)\right]$$

Here, I_{bg} is the background intensity, b is a pre-factor indicating the conversion efficiency, erf is the error function, $x_1$and x_2 are the beginning and the end of the converted region and D is the diffusion constant. Fitting this model to the time evolution of the intensity allows to track the lateral velocity of the photoconverted area, which was found to be close to 0 independent of whether a bleb formed or not (Figure 2C). This approach does also provide the diffusion constant of the Dendra2-F protein which, was found to be $D = 1.8 \pm 0.7 \frac{\mu m^2}{s}$ (mean ± std, n=8), comparable to the diffusion constant of other membrane bound proteins (Goehring et al., 2010).

Confocal imaging of fixed PGCs—Embryos of transgenic line *Tg(kop:mCherry-f-UTRnanos3)* were fixed at 8hpf in 2% PFA for 2 hours and imaged using Zeiss LSM-710 confocal microscope equipped with 63× water-immersion objective with NA=1,0 pinhole 1AU and 1 μm optical slices. Images were analyzed using Fiji software.

Manipulations of medium osmolarity—7–9hpf embryos from *Tg(kop:mCherry-f-UTRnanos3)* transgenic line were de-yolked manually (see movie 1 in (Goudarzi et al., 2015). The embryos were then maintained in 1% low melting point agarose (Invitrogen) covered with Leibovitz's L-15 as iso-osmotic medium (Gibco). Frames were captured at 5 sec intervals on a confocal spinning disk microscope for up to 30min. Hypo-osmotic treatment was induced by replacing the medium with distilled water, while the hyper-osmotic treatment was induced by exchange of the medium with a 2osmol NaCl solution. The circumference of the cells was measured manually using Fiji freehand tool.

Circumference measurement of Teneo VolumeScope data—A VolumeScope SEM picture per 200nm was selected for analysis. Multiple lines were drawn either precisely following the plasma membrane contours (detailed measurement), or by mimicking the resolution of light microscopy and ignoring small folds (coarse measurement). These measurements were performed for two PGCs (29 slices (example A) and 15 slices (example B)). For each type of measurement (detailed and course) the total length of the lines was measured and the ratio between them was determined.

BAR domain expression in PGCs—The N-BAR domain of human Amphiphysin and Nadrin fused to YFP was expressed in PGCs by injection of 50pg mRNA into 1-cell stage embryos. A 1 μm^2 region of interest was used for measuring the mean label intensity. For overexpression of the N-BAR protein, 250pg of the Amphiphysin-encoding RNA were injected and the migration and morphology of PGCs examined.

Generation of non ligand binding non internalizable CXCR4b—A truncation (amino acids 15 to 25) in region of ligand binding site of CXCR4b (Veldkamp et al., 2008)

was generated rendering the protein inactive in cell guidance in addition to a truncation in the c-terminal part of the molecule that inhibits internalization of the receptor (Minina et al., 2007). This molecule was used in the photobleaching experiments.

Filopodia length measurement—Length of the filopodia was measured before and after bleb inflation using the Freehand tool of Fiji.

Labeling PGCs' plasma membrane lipids—Embryos from 9hpf *Tg(kop:EGFP-LIFEACT-UTRnanos3)* transgenic line where deyolked in Leibovitz's L-15 (Gibco) medium (see movie 1 in (Goudarzi et al., 2015). Embryos were then transferred to a drop of 1% low melting point agarose (Invitrogen) containing 0.4 mM FM4-64 (Thermo Fisher Scientific). Imaging was performed using a Zeiss LSM710 confocal microscope (three Z-planes within a focal depth of 4 μm were captured every 2,5sec for 50 time points). The data presented in the Figure S1E, are derived from a maximum projection of the 3 Z-planes. The minimum and maximum intensity values in expanded blebs and pre-bleb membranes were determined as follows – a line tracing the membrane was drawn and signal intensity was measured for $1\mu m^2$ blocks along it. The maximum and minimum block intensity values were then determined for each membrane region. The values presented in the graph are the ratios between the maximum intensity measured in the expanded bleb and that in the pre-bleb (Fig. S1E, left). Similarly, the ratios between the minimum intensity measured in the expanded bleb and that measured in the pre-bleb are presented (Fig. S1E, right).

Photobleaching—For bleaching of the cell plasma membrane, a line-bleach (15-pixel width (3.5 μm)) was defined in Visi-View software. Bleaching was performed using a spinning-disk confocal microscope employing 10% (7mW) power 405nm laser and 63× water-immersion objective NA=1.0. Due to variability in the depth of the cells within the embryo and the position within the microscope field, the precise laser power reaching the cell membrane differs significantly between experiments. This variability leads to bleaching of the fluorophore in a very large membrane area or conversely to no effect. For this reason, successful informative photoconversion and photobleaching was achieved in 20% of the trials.

Cytoplasmic intensity measurement upon bleb—Intensity of cytoplasmic GFP was measured using a circular region (2μm radius) before and after bleb inflation. The ratio was determined by dividing the bleb value by the pre-bleb value.

Whole-mount *in situ* hybridization—Two-color whole-mount chromogenic *in situ* hybridization was performed as described previously (Thisse and Thisse, 2008). Briefly, embryos were fixed in 4% PFA in PBS for 48 hours at 8°C, hand dechorionated and stored in 100% MeOH at −20°C. Embryos were permeabilized using 10 μg/ml Proteinase K (Roche) in PBT (1× PBS + 0.1% Tween) for 30 sec and fixed again for 1 hour. Hybridization was performed using Digoxigenin-labeled *nanos3* [GenBank: NM_131878] and fluorescein-labeled *caveolin1* [GenBank: NM_212651] probes were synthetized according to the manufacturer's protocol (Roche, Switzerland). Detection of the probes was performed sequentially by incubating the embryos with an anti-Digoxigenin or anti-Fluorescein antibody coupled to alkaline phosphase (Roche) diluted 1:5000 and 1:10000 respectively in

blocking solution (0.1% Tween in PBS, 2% sheep serum, 2 mg/ml BSA). Removal of the first antibody was achieved in 0.1M glycine, pH 2.2, for 10 min. The staining reaction was performed using either NBT/BCIP (Roche, blue staining) or INT/BCIP (Roche, red staining) in NTMT buffer (100mM Tris HCl pH 9.5, 50mM $MgCl_2$, 100mM NaCl, 0.1% Tween). Images were captured on an Axioplan2 microscope (Zeiss) using a SPOT Xplorer camera (SPOT Imaging Solutions) controlled by Metamorph (Visitron Systems) software and processed using ImageJ (NIH).

CLEM on PGCs and VolumeScope—For localization of PGCs in the tissue in electron microscopy analysis, the samples were initially fixed in 2 % paraformaldehyde, 0.2 % glutaraldehyde in 0.1 M PHEM-buffer. As the germ cells are a very rare population (about 0.2% of the cells in the embryo at this stage) we relied on the GFP signal for locating the cells as presented in (Goudarzi et al., 2015). Employing higher glutaraldehyde concentration initially would eliminate the GFP signal in the cells, preventing their identification and analysis by EM. We then employed a laser-marking technique (arrow in Figure 3) to label the position of PGCs. Following the 2 % paraformaldehyde, 0.2 % glutaraldehyde fixation the samples were re-fixed in a solution of 2% paraformaldehyde, 2% glutaraldehyde.

Subsequently, the samples were fixed again, including thiocarbohydrazide and osmium tetroxide in the solution, as required for the imaging of serial block face scanning electron microscopy (Deerinck et al., 2010). The sample was then dehydrated and embedded in Epon. The region of interest was sectioned using an ultramicrotome (UC6, Leica, Austria). The sample was glued to a VolumeScope stub (Agar Scientific) and grounded with silver paint and a thin layer of platinum. Serial block face scanning electron microscopy was performed on Teneo VolumeScope (FEI, Eindhoven, the Netherlands), operating in low vacuum mode (50 Pa; water vapor). 500 images were acquired every 20 nm with a 10 nm × 10 nm pixel size.

QUANTIFICATION AND STATISTICAL ANALYSIS

Statistical analysis was performed using GraphPad Prism 6 software, or using Microsoft Excel. All graphs depict median and interquartile range values.

DATA AND SOFTWARE AVAILABILITY

All relevant data are available as ZIP files named Radial_analysis and Postprocess _Analysis that can be downloaded from - http://dx.doi.org/10.17632/wmtzc7w3d7.2 .

Supplementary Material

Refer to Web version on PubMed Central for supplementary material.

Acknowledgments

This work was supported by the European Research Council (ERC, CellMig, N 268806), the Deutsche Forschungsgemeinschaft (DFG, RA863/11-1), and the IZKF Muenster (Raz2/021/16) to E.R., the Cells in Motion cluster of excellence (EXC 1003-CIM) to E.R. T.B. and M.G. and NIH (AR065439) to M.B.

We thank Nina Knubel for the design of the graphical abstract. We thank the FEI Company (Eindhoven, the Netherlands) for their kind support in recording the Teneo VolumeScope data, especially to Ingo Gestmann and Liesbeth Hekking.

References

Akeda Y, Kodama T, Kashimoto T, Cantarelli V, Horiguchi Y, Nagayama K, Iida T, Honda T. Dominant-negative Rho, Rac, and Cdc42 facilitate the invasion process of Vibrio parahaemolyticus into Caco-2 cells. Infect Immun. 2002; 70:970–973. [PubMed: 11796633]

Arbizzani F, Mayrhofer M, Mione M. Novel transgenic lines to fluorescently label clathrin and caveolin endosomes in live zebrafish. Zebrafish. 2015; 12:202–203. [PubMed: 25748563]

Barton LJ, LeBlanc MG, Lehmann R. Finding their way: themes in germ cell migration. Curr Opin Cell Biol. 2016; 42:128–137. [PubMed: 27484857]

Blaser H, Eisenbeiss S, Neumann M, Reichman-Fried M, Thisse B, Thisse C, Raz E. Transition from non-motile behaviour to directed migration during early PGC development in zebrafish. J Cell Sci. 2005; 118:4027–4038. [PubMed: 16129886]

Blaser H, Reichman-Fried M, Castanon I, Dumstrei K, Marlow FL, Kawakami K, Solnica-Krezel L, Heisenberg CP, Raz E. Migration of zebrafish primordial germ cells: a role for myosin contraction and cytoplasmic flow. Dev Cell. 2006; 11:613–627. [PubMed: 17084355]

Cao J, Navis A, Cox BD, Dickson AL, Gemberling M, Karra R, Bagnat M, Poss KD. Single epicardial cell transcriptome sequencing identifies Caveolin 1 as an essential factor in zebrafish heart regeneration. Development. 2016; 143:232–243. [PubMed: 26657776]

Charras G, Paluch E. Blebs lead the way: how to migrate without lamellipodia. Nat Rev Mol Cell Biol. 2008; 9:730–736. [PubMed: 18628785]

Charras GT, Coughlin M, Mitchison TJ, Mahadevan L. Life and times of a cellular bleb. Biophysical journal. 2008; 94:1836–1853. [PubMed: 17921219]

Chavrier P, Parton RG, Hauri HP, Simons K, Zerial M. Localization of low molecular weight GTP binding proteins to exocytic and endocytic compartments. Cell. 1990; 62:317–329. [PubMed: 2115402]

Deerinck TJ, Bushong EA, Thor A, Ellisman MH. NCMIR methods for 3D EM: A new protocol for preparation of biological specimens for serial block face scanning electron microscopy. Microscopy (online). 2010:6–8.

Diz-Munoz A, Romanczuk P, Yu W, Bergert M, Ivanovitch K, Salbreux G, Heisenberg CP, Paluch EK. Steering cell migration by alternating blebs and actin-rich protrusions. BMC Biol. 2016; 14:74. [PubMed: 27589901]

Drab M, Verkade P, Elger M, Kasper M, Lohn M, Lauterbach B, Menne J, Lindschau C, Mende F, Luft FC, et al. Loss of caveolae, vascular dysfunction, and pulmonary defects in caveolin-1 gene-disrupted mice. Science. 2001; 293:2449–2452. [PubMed: 11498544]

Driscoll MK, Danuser G. Quantifying Modes of 3D Cell Migration. Trends in Cell Biology. 2015; 25:749–759. [PubMed: 26603943]

Fackler OT, Grosse R. Cell motility through plasma membrane blebbing. J Cell Biol. 2008; 181:879–884. [PubMed: 18541702]

Fehon RG, McClatchey AI, Bretscher A. Organizing the cell cortex: the role of ERM proteins. Nat Rev Mol Cell Biol. 2010; 11:276–287. [PubMed: 20308985]

Figard L, Wang M, Zheng L, Golding I, Sokac AM. Membrane Supply and Demand Regulates F-Actin in a Cell Surface Reservoir. Dev Cell. 2016; 37:267–278. [PubMed: 27165556]

Figard L, Xu H, Garcia HG, Golding I, Sokac AM. The plasma membrane flattens out to fuel cell-surface growth during Drosophila cellularization. Dev Cell. 2013; 27:648–655. [PubMed: 24316147]

Friedl P, Wolf K. Plasticity of cell migration: a multiscale tuning model. J Cell Biol. 2010; 188:11–19. [PubMed: 19951899]

Frost A, Unger VM, De Camilli P. The BAR domain superfamily: membrane-molding macromolecules. Cell. 2009; 137:191–196. [PubMed: 19379681]

Galic M, Jeong S, Tsai FC, Joubert LM, Wu YI, Hahn KM, Cui Y, Meyer T. External push and internal pull forces recruit curvature-sensing N-BAR domain proteins to the plasma membrane. Nat Cell Biol. 2012; 14:874–881. [PubMed: 22750946]

Garcia J, Bagwell J, Njaine B, Norman J, Levic DS, Wopat S, Miller SE, Liu X, Locasale JW, Stainier DYR, et al. Sheath Cell Invasion and Trans-differentiation Repair Mechanical Damage Caused by Loss of Caveolae in the Zebrafish Notochord. Curr Biol. 2017

Gauthier NC, Fardin MA, Roca-Cusachs P, Sheetz MP. Temporary increase in plasma membrane tension coordinates the activation of exocytosis and contraction during cell spreading. Proc Natl Acad Sci U S A. 2011; 108:14467–14472. [PubMed: 21808040]

Gervasio OL, Phillips WD, Cole L, Allen DG. Caveolae respond to cell stretch and contribute to stretch-induced signaling. Journal of cell science. 2011; 124:3581–3590. [PubMed: 22045729]

Goehring NW, Chowdhury D, Hyman AA, Grill SW. FRAP analysis of membrane-associated proteins: lateral diffusion and membrane-cytoplasmic exchange. Biophys J. 2010; 99:2443–2452. [PubMed: 20959084]

Goudarzi M, Banisch TU, Mobin MB, Maghelli N, Tarbashevich K, Strate I, van den Berg J, Blaser H, Bandemer S, Paluch E, et al. Identification and regulation of a molecular module for bleb-based cell motility. Developmental cell. 2012; 23:210–218. [PubMed: 22705393]

Goudarzi M, Mildner K, Babatz F, Riedel D, Klambt C, Zeuschner D, Raz E. Correlative Light and Electron Microscopy of Rare Cell Populations in Zebrafish Embryos Using Laser Marks. Zebrafish. 2015; 12:470–473. [PubMed: 26448280]

Hallett MB, Dewitt S. Ironing out the wrinkles of neutrophil phagocytosis. Trends in cell biology. 2007; 17:209–214. [PubMed: 17350842]

Heasman SJ, Ridley AJ. Mammalian Rho GTPases: new insights into their functions from in vivo studies. Nat Rev Mol Cell Biol. 2008; 9:690–701. [PubMed: 18719708]

Hopkins CR, Gibson A, Shipman M, Strickland DK, Trowbridge IS. In migrating fibroblasts, recycling receptors are concentrated in narrow tubules in the pericentriolar area, and then routed to the plasma membrane of the leading lamella. J Cell Biol. 1994; 125:1265–1274. [PubMed: 7515888]

Inoue M, Chang L, Hwang J, Chiang SH, Saltiel AR. The exocyst complex is required for targeting of Glut4 to the plasma membrane by insulin. Nature. 2003; 422:629–633. [PubMed: 12687004]

Kabaso D, Shlomovitz R, Schloen K, Stradal T, Gov NS. Theoretical model for cellular shapes driven by protrusive and adhesive forces. PLoS Comput Biol. 2011; 7:e1001127. [PubMed: 21573201]

Kabeche R, Howard L, Moseley JB. Eisosomes provide membrane reservoirs for rapid expansion of the yeast plasma membrane. J Cell Sci. 2015; 128:4057–4062. [PubMed: 26403204]

Kapustina M, Elston TC, Jacobson K. Compression and dilation of the membrane-cortex layer generates rapid changes in cell shape. J Cell Biol. 2013; 200:95–108. [PubMed: 23295349]

Kardash E, Reichman-Fried M, Maitre JL, Boldajipour B, Papusheva E, Messerschmidt EM, Heisenberg CP, Raz E. A role for Rho GTPases and cell-cell adhesion in single-cell motility in vivo. Nat Cell Biol. 2010; 12:47–53. sup pp 41–11. [PubMed: 20010816]

Karotki L, Huiskonen JT, Stefan CJ, Ziolkowska NE, Roth R, Surma MA, Krogan NJ, Emr SD, Heuser J, Grunewald K, et al. Eisosome proteins assemble into a membrane scaffold. J Cell Biol. 2011; 195:889–902. [PubMed: 22123866]

Keller H, Eggli P. Protrusive activity, cytoplasmic compartmentalization, and restriction rings in locomoting blebbing Walker carcinosarcoma cells are related to detachment of cortical actin from the plasma membrane. Cell Motil Cytoskeleton. 1998; 41:181–193. [PubMed: 9786092]

Kleinschmidt JH. Folding kinetics of the outer membrane proteins OmpA and FomA into phospholipid bilayers. Chem Phys Lipids. 2006; 141:30–47. [PubMed: 16581049]

Kosmalska AJ, Casares L, Elosegui-Artola A, Thottacherry JJ, Moreno-Vicente R, Gonzalez-Tarrago V, del Pozo MA, Mayor S, Arroyo M, Navajas D, et al. Physical principles of membrane remodelling during cell mechanoadaptation. Nat Commun. 2015; 6:7292. [PubMed: 26073653]

Kwok R, Evans E. Thermoelasticity of large lecithin bilayer vesicles. Biophysical Journal. 1981; 35:637–652. [PubMed: 7272454]

Lammermann T, Sixt M. Mechanical modes of ‘amoeboid’ cell migration. Current opinion in cell biology. 2009; 21:636–644. [PubMed: 19523798]

Laster SM, Mackenzie JM Jr. Bleb formation and F-actin distribution during mitosis and tumor necrosis factor-induced apoptosis. Microscopy research and technique. 1996; 34:272–280. [PubMed: 8743415]

Masters TA, Pontes B, Viasnoff V, Li Y, Gauthier NC. Plasma membrane tension orchestrates membrane trafficking, cytoskeletal remodeling, and biochemical signaling during phagocytosis. Proc Natl Acad Sci U S A. 2013; 110:11875–11880. [PubMed: 23821745]

Mayor S, Parton RG, Donaldson JG. Clathrin-independent pathways of endocytosis. Cold Spring Harb Perspect Biol. 2014:6.

Meyen D, Tarbashevich K, Banisch TU, Wittwer C, Reichman-Fried M, Maugis B, Grimaldi C, Messerschmidt EM, Raz E. Dynamic filopodia are required for chemokine-dependent intracellular polarization during guided cell migration in vivo. Elife. 2015:4.

Minina S, Reichman-Fried M, Raz E. Control of receptor internalization, signaling level, and precise arrival at the target in guided cell migration. Curr Biol. 2007; 17:1164–1172. [PubMed: 17600713]

Nassoy P, Lamaze C. Stressing caveolae new role in cell mechanics. Trends in cell biology. 2012; 22:381–389. [PubMed: 22613354]

Norman LL, Brugues J, Sengupta K, Sens P, Aranda-Espinoza H. Cell blebbing and membrane area homeostasis in spreading and retracting cells. Biophys J. 2010; 99:1726–1733. [PubMed: 20858416]

Paksa A, Raz E. Zebrafish germ cells: motility and guided migration. Current Opinion in Cell Biology. 2015; 36:80–85. [PubMed: 26232877]

Paluch E, Piel M, Prost J, Bornens M, Sykes C. Cortical actomyosin breakage triggers shape oscillations in cells and cell fragments. Biophys J. 2005; 89:724–733. [PubMed: 15879479]

Paluch EK, Raz E. The role and regulation of blebs in cell migration. Current Opinion in Cell Biology. 2013; 25:582–590. [PubMed: 23786923]

Peter BJ, Kent HM, Mills IG, Vallis Y, Butler PJ, Evans PR, McMahon HT. BAR domains as sensors of membrane curvature: the amphiphysin BAR structure. Science. 2004; 303:495–499. [PubMed: 14645856]

Reichman-Fried M, Minina S, Raz E. Autonomous modes of behavior in primordial germ cell migration. Developmental cell. 2004; 6:589–596. [PubMed: 15068797]

Ren M, Xu G, Zeng J, De Lemos-Chiarandini C, Adesnik M, Sabatini DD. Hydrolysis of GTP on rab11 is required for the direct delivery of transferrin from the pericentriolar recycling compartment to the cell surface but not from sorting endosomes. Proc Natl Acad Sci U S A. 1998; 95:6187–6192. [PubMed: 9600939]

Sabharanjak S, Sharma P, Parton RG, Mayor S. GPI-anchored proteins are delivered to recycling endosomes via a distinct cdc42-regulated, clathrin-independent pinocytic pathway. Dev Cell. 2002; 2:411–423. [PubMed: 11970892]

Sens P, Plastino J. Membrane tension and cytoskeleton organization in cell motility. J Phys Condens Matter. 2015; 27:273103. [PubMed: 26061624]

Sheetz MP, Sable JE, Dobereiner HG. Continuous membrane-cytoskeleton adhesion requires continuous accommodation to lipid and cytoskeleton dynamics. Annu Rev Biophys Biomol Struct. 2006; 35:417–434. [PubMed: 16689643]

Sinha B, Koster D, Ruez R, Gonnord P, Bastiani M, Abankwa D, Stan RV, Butler-Browne G, Vedie B, Johannes L, et al. Cells respond to mechanical stress by rapid disassembly of caveolae. Cell. 2011; 144:402–413. [PubMed: 21295700]

Small JV, Stradal T, Vignal E, Rottner K. The lamellipodium: where motility begins. Trends Cell Biol. 2002; 12:112–120. [PubMed: 11859023]

Spiczka KS, Yeaman C. Ral-regulated interaction between Sec5 and paxillin targets Exocyst to focal complexes during cell migration. J Cell Sci. 2008; 121:2880–2891. [PubMed: 18697830]

Stenmark H, Parton RG, Steele-Mortimer O, Lutcke A, Gruenberg J, Zerial M. Inhibition of rab5 GTPase activity stimulates membrane fusion in endocytosis. EMBO J. 1994; 13:1287–1296. [PubMed: 8137813]

Strychalski W, Guy RD. A computational model of bleb formation. Math Med Biol. 2013; 30:115–130. [PubMed: 22294562]

Takahashi S, Kubo K, Waguri S, Yabashi A, Shin HW, Katoh Y, Nakayama K. Rab11 regulates exocytosis of recycling vesicles at the plasma membrane. J Cell Sci. 2012; 125:4049–4057. [PubMed: 22685325]

Taloni A, Kardash E, Salman OU, Truskinovsky L, Zapperi S, La Porta CA. Volume Changes During Active Shape Fluctuations in Cells. Phys Rev Lett. 2015; 114:208101. [PubMed: 26047252]

Tarbashevich K, Reichman-Fried M, Grimaldi C, Raz E. Chemokine-Dependent pH Elevation at the Cell Front Sustains Polarity in Directionally Migrating Zebrafish Germ Cells. Curr Biol. 2015; 25:1096–1103. [PubMed: 25843033]

Veldkamp CT, Seibert C, Peterson FC, De la Cruz NB, Haugner JC 3rd, Basnet H, Sakmar TP, Volkman BF. Structural basis of CXCR4 sulfotyrosine recognition by the chemokine SDF-1/CXCL12. Sci Signal. 2008; 1:ra4. [PubMed: 18799424]

Welch MD. Cell migration, freshly squeezed. Cell. 2015; 160:581–582. [PubMed: 25679757]

Zanchi R, Howard G, Bretscher MS, Kay RR. The exocytic gene secA is required for Dictyostelium cell motility and osmoregulation. J Cell Sci. 2010; 123:3226–3234. [PubMed: 20807800]

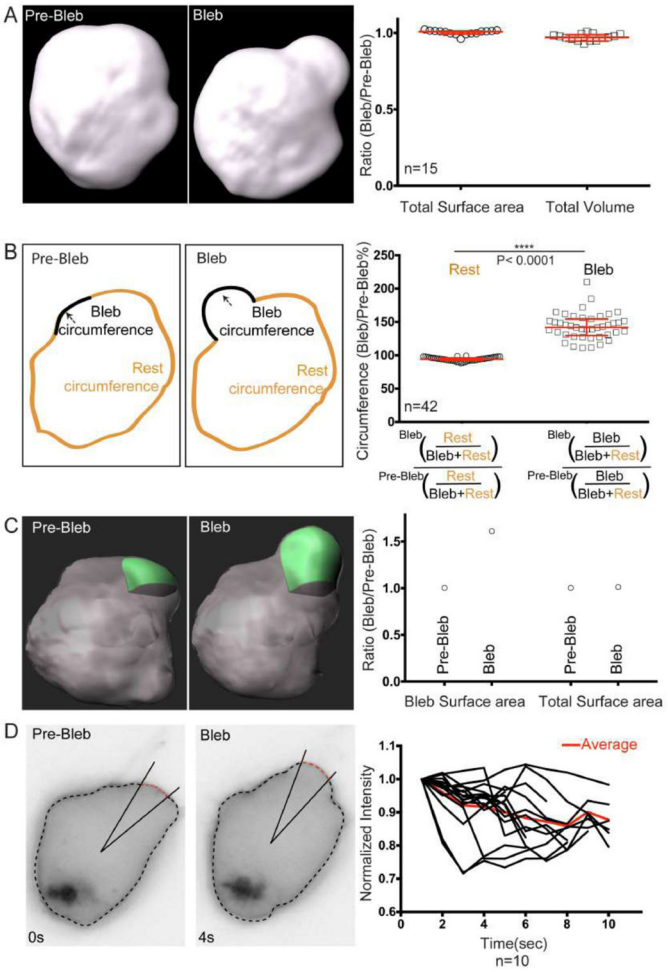

Figure 1. Cell shape and membrane characteristics during bleb inflation *in vivo*

(**A**) 3D reconstruction showing a PGC before and after bleb inflation. The graph on the right shows the ratio of the cell surface area and the volume comparing Bleb to the Pre-Bleb time points. (**B**) Schematic view of a PGC circumference prior to and following bleb formation, with black and orange colors representing the measured areas. The graph shows the ratio between the circumference of cells excluding the bleb area before and after bleb expansion (normalized to the whole cell circumference) and the same ratio for the bleb area (Median= 94.1 and 141.8 percent for ‘Rest’ and ‘Bleb’, respectively). The circumference of the bleb prior to inflation was defined as the membrane length of the bleb neck at the Pre-bleb time point. (**C**) 3D surface reconstruction for bleb (green) and the whole cell (grey) prior and after bleb expansion. The graph on the right shows the change in surface area of the bleb and the whole cell, before (Pre-Bleb) and after bleb expansion (Bleb). (**D**) A PGC expressing farnesylated GFP protein prior to and following bleb inflation. The cell outline was calculated using Radial-analysis program (see Methods) and the bleb was defined by the change in the velocity of the plasma membrane. The central half of the bleb region (red dashed line) was monitored over time and the fluorescence intensities were plotted (right). The average intensity obtained from 10 measurements is presented in red. The graphs in **A** and **B** show median and interquartile range for data obtained in 3 independent experiments.

The P value was calculated using non-parametric Mann Whitney U test. See also Figure S6. n represents the number of bleb analyzed. In all of the panels the PGC membrane was labeled with farnesylated GFP.

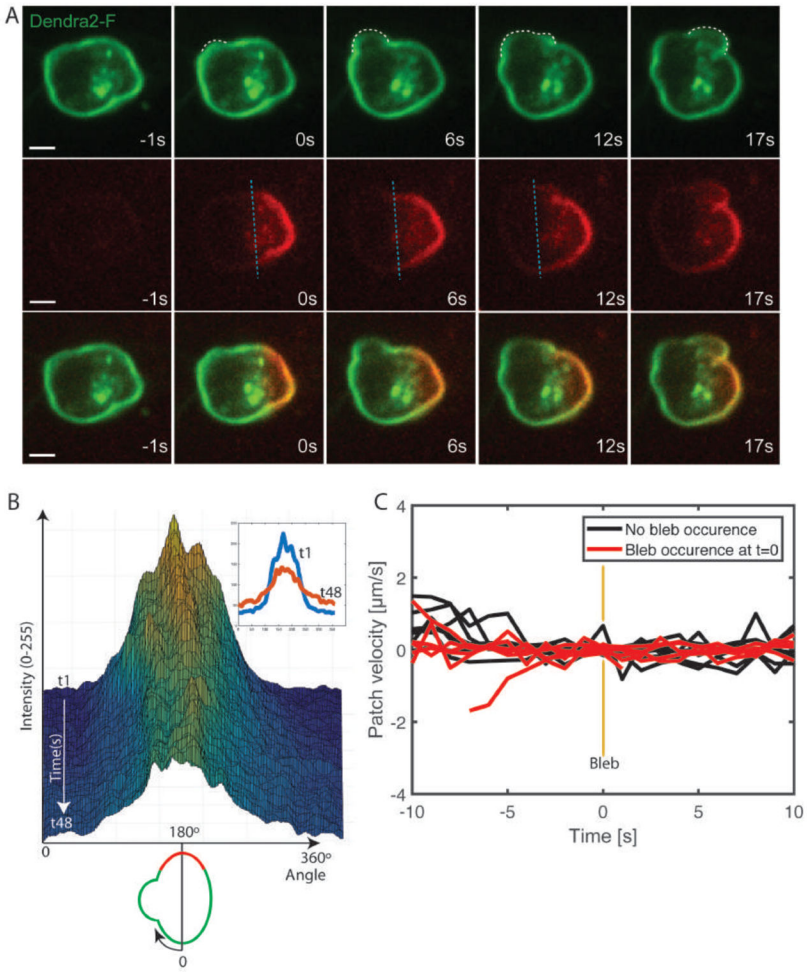

Figure 2. Lack of membrane flow in the direction of the forming bleb in PGCs migrating within live embryos

(**A**) Farnesylated-Dendra2 (Dendra2-F) expressed on the plasma membrane of PGCs from 7–8 hpf embryos was photoconverted (green to red) at the border of a forming bleb (White dashed line shows the contours of two sequential blebs, with the blue dashed line marking the edge of the converted area up to the 12s time point). Cells were imaged at a frequency of one time-point per second and the photoconversion time point is presented as zero (0s). No directional flow with respect to the forming bleb is observed. 7 events of photoconversion next to a forming bleb were analyzed. Scale bar= 5μm (**B**) The 3D surface plot of the converted area showing the intensity change along the circumference (0°–360°) of the cell presented in panel A, over 48 seconds, but no change in the position of the center of the converted area. The inset shows the circumferential intensity in the first (1 second) and the last frame after photoconversion (48 seconds). A schematic drawing of the cell analyzed is presented below the X-axis. (**C**) A graph showing the velocity of the center of the photoconverted region in cells where blebs did not form (n=5, black) and in cells in which bleb inflation occurred next to the photoconverted area (n=7, red). t0 is the time of bleb formation. See also Figure S1.

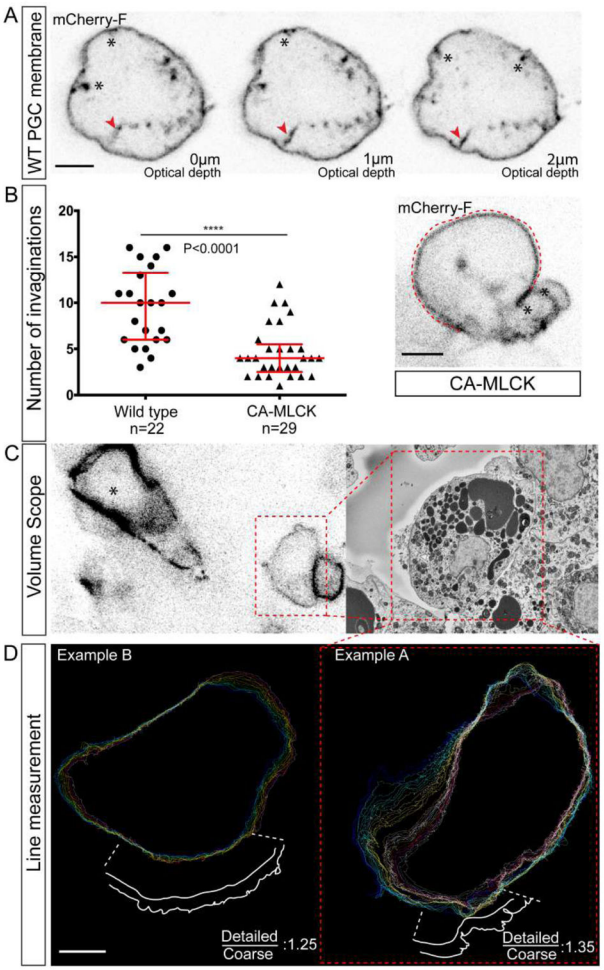

Figure 3. Detailed analysis of PGCs within the tissue reveals membrane invaginations

(**A**) Three confocal planes of a PGC plasma membrane labeled with Farnesylated-mCherry providing a z-axis view of invaginations extending into the cell interior. One such invagination is highlighted with a red arrowhead at each of the 3 planes. Note that in the first plane, the connection of the structure to the membrane is not clearly seen, such that it resembles a vesicle. Additional invaginations connected to the plasma membrane are marked with black asterisks. (**B**) The graph shows the number of membrane invaginations in wild-type PGCs and in PGCs with elevated contractility (CA-MLCK), with an example for a manipulated cell presented on the right (n= 22 and 29 cells from 6 and 19 embryos, respectively. The graph shows the combined data from two independent experiments). The red dashed line highlights the contour of a large travelling bleb with black asterisks marking membrane invaginations within the cell body (see also Movie S4D). The P value is calculated using non-parametric Mann Whitney test. (**C**) Localization of PGCs for the correlative electron microscopy analysis, employing an arrowhead-shaped laser mark (asterisk). The dashed area labels one of the PGCs studied in the Teneo VolumeScope (right panel). (**D**) The Teneo VolumeScope data was used to measure the extent of extra plasma membrane stored in invaginations and wrinkles in PGCs (excluding long membrane tubes that span multiple planes). Every 200nm, the circumference of the cell was outlined, either

by following the invaginations and wrinkles precisely, or by crude tracing of the cell circumference (see example in the magnified region at the bottom). The ratio between the circumference lengths obtained using the detailed Teneo VolumeScope data and the coarse estimate for two cells is presented (29 and 15 sections were used for example A and B respectively). Scale Bars = 5 μm. See also Figure S2.

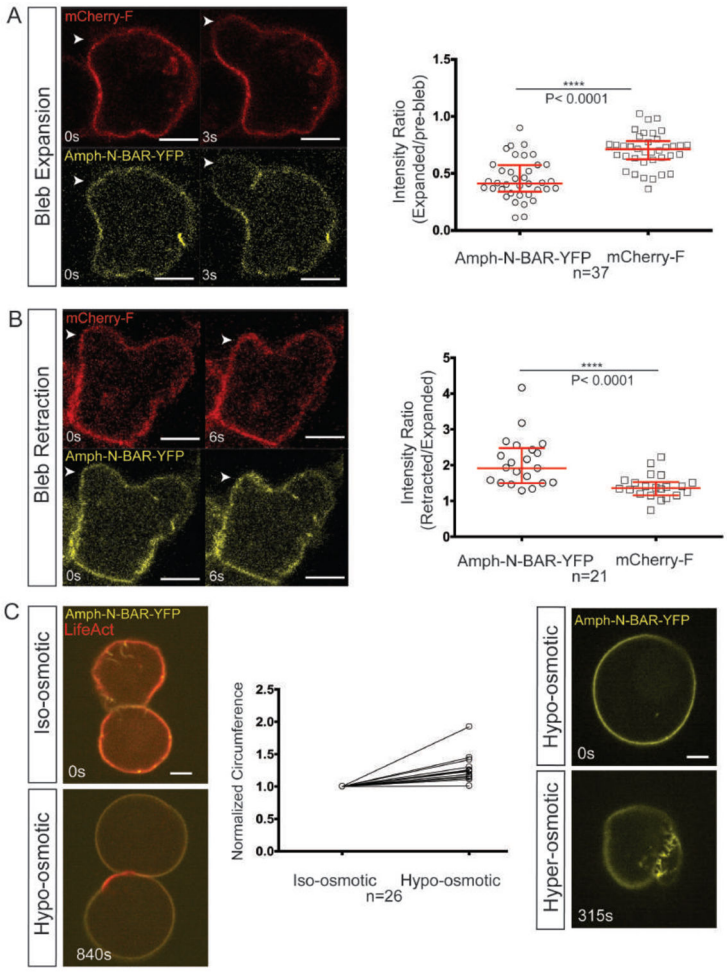

Figure 4. Analysis of plasma membrane invaginations unfolding and folding during bleb inflation and retraction

(**A**) The YFP-labeled N-BAR domain of Amphiphysin interacts with the plasma membrane and marks membrane structures protruding into the cytoplasm and the mCherry-F protein labels the PGC's plasma membrane. White arrowheads point at the position of bleb expansion. The graph on the right shows that the signal intensity of the BAR domain (Amph-N-BAR-YFP) on the plasma membrane is reduced upon bleb expansion, with a smaller reduction observed using the farnesylated mCherry (mCherry-F) probe. (Median= 0.41 and 0.71 for the N-BAR probe and the mCherry-F, respectively, n=37 cells from 21 embryos) (**B**) A similar analysis to that in (A) was conducted during bleb retraction. White arrowheads point at the position of bleb retraction. The graphs present the intensity ratio of each of the two probes, Amph-N-BAR-YFP and mCherry-F, between the retracted bleb and the expanded bleb. (Median= 1.91 and 1.35 for the N-BAR probe and the mCherry-F, respectively, n=21 cells from 15 embryos). (**C**) Two PGCs in deyolked embryos expressing N-BAR domain of Amphiphysin and lifeAct in an Iso-osmotic (Left, upper panel) and later in Hypo-osmotic conditions (left, lower panel). The graph shows the change in the circumference of the cells in a confocal section after the exposure to hypo-osmotic medium. The values are normalized to the circumference in the iso-osmotic solution (n=26 cells).

Right panels show a PGC expressing N-BAR domain of Amphiphysin (Amph-N-BAR-YFP) subjected to a change from Hypo-osmotic to Hyper-osmotic conditions (right, upper and lower panels respectively). All graphs show median and interquartile range. The P value is calculated using non-parametric Mann Whitney test. Scale bars = 5μm. See also Figure S3 and S4.

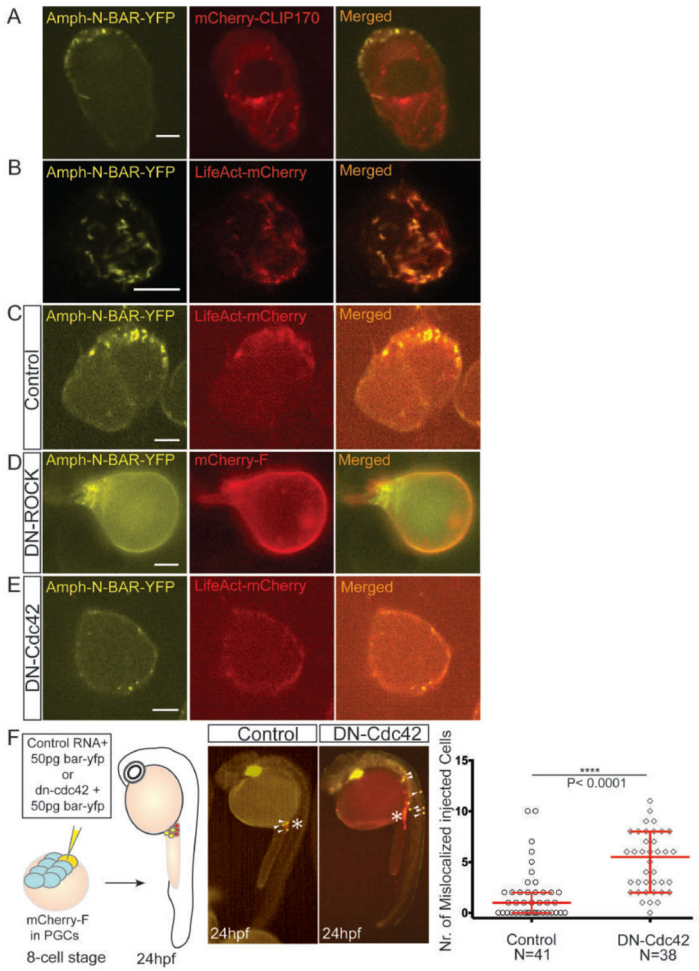

Figure 5. Membrane invaginations in PGCs migrating within live embryos require Cdc42 for formation and colocalize with polymerized actin structures

(**A**) Lack of co-localization between membrane invaginations labeled by Amph-N-BAR-YFP and microtubules labeled with mCherry-CLIP170. (**B**) Confocal images of membrane invaginations labeled with the Amph-N-BAR-YFP protein and their co-localization with polymerized actin labeled with LifeAct-mCherry protein. The cell orientation is such that the front is facing the lens. (**C**) Co-localization of membrane invaginations in polarized PGCs labeled by Amph-N-BAR-YFP with polymerized actin labeled with LifeAct-mCherry protein. Cell front facing upper right. (**D**) Membrane invaginations labeled with the Amph-N-BAR-YFP protein in cells in which contractility was inhibited by the expression of a dominant-negative form of ROCK (DN-ROCK). mCherry-F labels the plasma membrane. (**E**) Dominant-negative form of Cdc42 (DN-Cdc42) expressed in the cells reduces the number of dynamic membrane invaginations labeled with Amph-N-BAR YFP. Polymerized actin is labeled with LifeAct-mCherry protein. (**F**) Inhibition of Cdc42 function in a fraction of the PGC population led to mislocalization of the treated cells (yellow cells). The asterisks mark the migration target of the cells in 24hpf embryos and the white arrowheads point at PGCs expressing a control or the DN-Cdc42 proteins. The graph shows the quantitation of the result (N=41 and 38 embryos from 2 independent experiments). Scale bars 5μm. Median

(1 and 5 respectively) and interquartile range are shown. P value was calculated using non-parametric Mann Whitney U test.

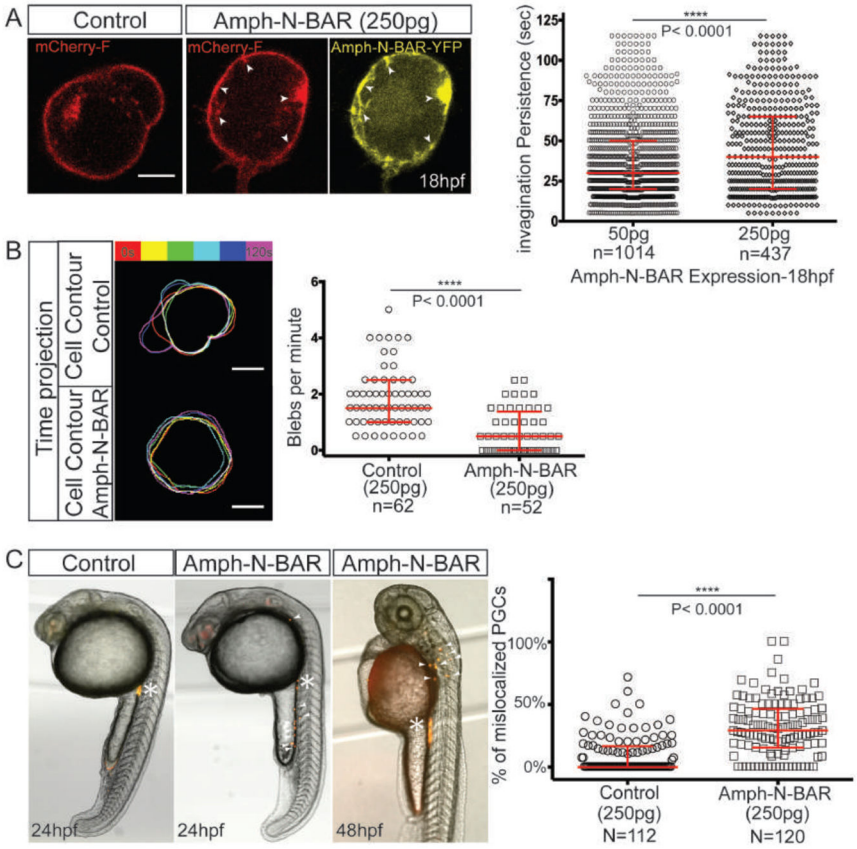

Figure 6. Release of membrane invaginations is required for cell blebbing *in vivo*

(**A**) The morphology of a wild-type PGC at 18hpf, injected with control RNA (left) and of a PGC expressing high levels of the Amphiphysin N-BAR domain (two right panels). Domains of increased plasma membrane accumulation (mCherry-F label, red) are observed at locations where high levels of YFP-tagged N-BAR domain protein (yellow) are present (arrowheads). The graph on the right presents the persistence of the invaginations as measured over 2 minutes under conditions of low (50pg, n=1014 in 28 cells) and high (250pg, n=437 in 33 cells) amounts of RNA injected per embryo. Three independent experiments were conducted with a median of 30 seconds (for 50pg) and 40 seconds (for 250pg). Scale bar= 5μm. (**B**) An overlay of 6 membrane contours (each 20 sec apart) of PGCs labeled with farnesylated-mCherry in control (250pg RNA, up) and in cells overexpressing the Amphiphysin N-BAR domain (250pg RNA, down), with the graph showing the number of blebs per minute (n is the number of cells analyzed, Median= 1.5 and 0.5 for control and N-BAR expression respectively). Scale bar= 5μm. (**C**) PGCs expressing high levels of the Amphiphysin N-BAR domain protein exhibit defects in arrival at the region where the gonad develops. Asterisk labels the migration target of PGCs in 24 and 48hpf embryos, and arrowheads point at some of the mislocalized PGCs. The graph presents the percentage of mislocalized PGCs in control and in PGCs expressing RNA encoding for the N-BAR domain protein (250 pg, N is the number of embryos analyzed) (Median= 0% and 29% for control and Amph-N-BAR respectively, data was obtained in 3 independent

experiments). The P value was calculated using non-parametric Mann Whitney U test. The graphs show median and interquartile range. See also Figure S5.

Key Resources Table

REAGENT or RESOURCE	SOURCE	IDENTIFIER
Antibodies		
Anti-Digoxigenin-AP, Fab fragments from sheep	Roche	Cat#11093274910; RRID:AB_514497
Anti-Fluorescein-AP, Fab fragments from sheep	Roche	Cat# 11426338910; RRID:AB_514504
Chemicals, Peptides, and Recombinant Proteins		
Glutaraldehyde solution, for electron microscopy, 25% in H2O	Sigma	G5882-10X1ML
FM4-64	ThermoFisher	Cat#T13320
UltraPure™ Low Melting Point Agarose	Invitrogen	Cat#16520100
Leibovitz's L-15 media	ThermoFisher	Cat# 31415-029
Critical Commercial Assays		
mMessage Machine kit	Ambion	Cat#AM1340
Deposited Data		
Post-process_analysis	This paper	Zip file at - https://doi.org/10.17632/wmtzc7w3d7.2
Radial analysis	This paper	Zip file at - https://doi.org/10.17632/wmtzc7w3d7.2
Experimental Models: Organisms/Strains		
Zebrafish: AB	Zebrafish International Resource Center (ZIRC	ZFIN: ZDB-GENO-960809-7
Zebrafish: Tg(*kop:EGFP-f-UTRnanos3*)	Blaser et al., 2006	ZDB-ALT-070406-1
Zebrafish: Tg(*kop:mCherry-f-UTR-nanos3*)	Tarbashevich et al., 2015	ZDB-ALT-150810-1
Zebrafish: Tg(kop:EGFP-LIFEACT-UTRnanos3)	Meyen et al., 2015	ZDB-ALT-141104-1
Zebrafish: cav3 pd1149	Garcia et al., 2017	ZDB-ALT-160405-5
Zebrafish: cav1 pd1104	Cao et al., 2016	ZDB-ALT-170907-1
Oligonucleotides		
RNA: 480: *cdc42* (T17N). *3′ nanos3UTR* (Dominant Negative)	This paper	N/A
RNA: 554: *cd14-3′ nanos3UTR*	This paper	N/A
RNA: 947: *zfrab5c (S36N)-3′ nanos3UTR* (Dominant Negative)	This paper	N/A
RNA: 949: *zfrab11a (S25N)-3′ nos1 UTR* (Dominant Negative)	This paper	N/A
RNA: A700: egfp-zfvamp8-*3′ nos1 UTR*	This paper	N/A
RNA: A801: *dsred-rab5c-3′ globin UTR*	This paper	N/A
RNA: A803: *zfrab11a-3′ globin UTR*	This paper	N/A
RNA: A279: *dsredex-[human beta 1, 4-galactosyltransferase]-3′ nos1UTR*	This paper	N/A
RNA: A741: *dn-zfexo70-3′ nanos3UTR* (Dominant Negative)	This paper	N/A
RNA: A918: *pa-gfp-3′ globin UTR*	This paper	N/A
RNA: B007: lifeact-Ruby-*3′ nanos3 UTR*	This paper	N/A
RNA: B790: *ca-zfmlck-3′ nanos3 UTR*	This paper	N/A

REAGENT or RESOURCE	SOURCE	IDENTIFIER
RNA: B854: *Δcxcr4b-egfp-3′ nanos3 UTR*	This paper	N/A
RNA: C229: *cav1a-egfp-3′ nanos3 UTR*	This paper	N/A
RNA: C504: *cav1a-egfp-3′ globin UTR*	This paper	N/A
RNA: C584: *mcherry-clip170h-3′ nanos3 UTR*	This paper	N/A
RNA: C944: *dendra2-f-3′ nanos3 UTR*	This paper	N/A
RNA: D333: *dn-exo70-3′ globin UTR* (Dominant Negative)	This paper	N/A
RNA: D597: *zfrab5c (S36N)-3′ globin UTR* (Dominant Negative)	This paper	N/A
RNA: D601: *zfrab11a (S25N)-3′ globin UTR* (Dominant Negative)	This paper	N/A
RNA: D617: *amph-nbar-yfp-3′ nanos3 UTR*	This paper	N/A
Software and Algorithms		
Graphpad	GraphPad Software, La Jolla California USA	https://www.graphpad.com/scientificsoftware/prism
Imaris, version 8.4.1, 2016	Bitplane Inc.	http://www.bitplane.com
Fiji	NIH	https://fiji.sc
ZEN software, versions 2010B SP1 (Release version 6.0 for LSM710) and 2014 SP1 (black edition, 64bit, Release version 9.0 for Lightsheet Z.1)	Zeiss	https://www.zeiss.com/microscopy/int/products/microscope-software/zen.html
VisiView, version 2.1.4, 2014	Visitron Systems GmbH	http://www.visitron.de/Products/Software/VisiView/visiview.html